



RESEARCH ARTICLE

Intracardiac MR imaging (ICMRI) guiding-sheath with amplified expandable-tip imaging and MR-tracking for navigation and arrhythmia ablation monitoring: Swine testing at 1.5 and 3T

Ehud J. Schmidt¹  | Gregory Olson² | Junichi Tokuda³ | Akbar Alipour¹  | Ronald D. Watkins⁴ | Eric M. Meyer¹ | Hassan Elahi¹ | William G. Stevenson⁵ | Jeffrey Schweitzer² | Charles L. Dumoulin⁶ | Thomas Johnson⁷ | Aravindan Kolandaivelu¹ | Wolfgang Loew⁶ | Henry R. Halperin¹

¹Medicine (Cardiology), Johns Hopkins University, Baltimore, Maryland, USA

²Cardiac Arrhythmia and Heart Failure Division, Abbott Laboratories, Minnetonka, Minnesota, USA

³Radiology, Brigham and Women's Hospital, Boston, Massachusetts, USA

⁴Radiology, Stanford University, Stanford, California, USA

⁵Cardiology, Brigham and Women's Hospital, Boston, Massachusetts, USA

⁶Radiology, Cincinnati Children's Hospital Medical Center, Cincinnati, Ohio, USA

⁷Catapult Product Development, Waltham, Massachusetts, USA

Correspondence

Ehud J. Schmidt, Medicine (Cardiology), Johns Hopkins University, Traylor 928, 1701 East Monument St, Baltimore, MD 21205, USA.
Email: eschmi17@jhu.edu

Funding information

National Institute of Biomedical Imaging and Bioengineering, Grant/Award Number: R01-EB020667; American Heart Association, Grant/Award Number: 10SDG261039; National Heart, Lung, and Blood Institute, Grant/Award Number: R01-HL094610, U41-RR019703 and U54-HL119145; Abbott Laboratories

Purpose: Develop a deflectable intracardiac MR imaging (ICMRI) guiding-sheath to accelerate imaging during MR-guided electrophysiological (EP) interventions for radiofrequency (500 kHz) ablation (RFA) of arrhythmia. Requirements include imaging at three to five times surface-coil SNR in cardiac chambers, vascular insertion, steerable-active-navigation into cardiac chambers, operation with ablation catheters, and safe levels of MR-induced heating.

Methods: ICMRI's 6 mm outer-diameter (OD) metallic-braided shaft had a 2.6 mm OD internal lumen for ablation-catheter insertion. Miniature-Baluns (MBaluns) on ICMRI's 1 m shaft reduced body-coil-induced heating. Distal section was a folded "star"-shaped imaging-coil mounted on an expandable frame, with an integrated miniature low-noise-amplifier overcoming cable losses. A handle-activated movable-shaft expanded imaging-coil to 35 mm OD for imaging within cardiac-chambers. Four MR-tracking micro-coils enabled navigation and motion-compensation, assuming a tetrahedron-shape when expanded. A second handle-lever enabled distal-tip deflection. ICMRI with a protruding deflectable EP catheter were used for MR-tracked navigation and RFA using a dedicated 3D-slicer user-interface. ICMRI was tested at 3T and 1.5T in swine to evaluate (a)

Previous-generation devices were presented at annual meetings: ISMRM 2016, 2017, SCMR 2015, and AHA 2010.

This is an open access article under the terms of the Creative Commons Attribution-NonCommercial-NoDerivs License, which permits use and distribution in any medium, provided the original work is properly cited, the use is non-commercial and no modifications or adaptations are made.

© 2022 The Authors. *Magnetic Resonance in Medicine* published by Wiley Periodicals LLC on behalf of International Society for Magnetic Resonance in Medicine.

heating, (b) cardiac-chamber access, (c) imaging field-of-view and SNR, and (d) intraprocedural RFA lesion monitoring.

Results: The 3T and 1.5T imaging SNR demonstrated >400% SNR boost over a $4 \times 4 \times 4 \text{ cm}^3$ FOV in the heart, relative to body and spine arrays. ICMRI with MBaluns met ASTM/IEC heating limits during navigation. Tip-deflection allowed navigating ICMRI and EP catheter into atria and ventricles. Acute-lesion long-inversion-time-T1-weighted 3D-imaging (TWILITE) ablation-monitoring using ICMRI required 5:30 min, half the time needed with surface arrays alone.

Conclusion: ICMRI assisted EP-catheter navigation to difficult targets and accelerated RFA monitoring.

KEYWORDS

acute RF lesion imaging, cardiac electrophysiology, interventional MRI

1 | INTRODUCTION

1.1 | MRI-guided interventional electrophysiology procedures and possible benefits of local coils

Intraprocedural MRI-guided electrophysiology (EP) procedures for the treatment of atrial fibrillation (AF) and ventricular tachycardia (VT) are currently in clinical trials in Europe.¹⁻³ radiofrequency ablation (RFA) is induced using 500 kHz inductive heating, which is delivered from cardiac catheters to disconnect the arrhythmia circuits. Intraprocedural MR-guidance aims to improve the success rate of conventional electrically-monitored RFA, which is currently only ~70% for paroxysmal AF and ~50% for VT and chronic AF.⁴⁻⁶ Symptom recurrence results, in part, from spatially incomplete ablation. MRI-guidance requires EP catheters be brought to locations selected from prior electroanatomic mapping (EAM), and RFA be performed with continuous MRI monitoring, validating that at each location, the thermal dose is sufficient to create burns which are deep and interconnected, so that arrhythmia does not recur post-procedurally. The topology of permanent (chronic, >4 weeks post-ablation) RFA lesions are reliably estimated with contrast-enhanced Late Gadolinium Enhancement contrast,^{7,8} but acute (short-term, <2 weeks) intraprocedural injury is overestimated.^{9,10} Therefore, non-contrast-enhanced 3D long-inversion-time (TI = 500–600 ms) T1-weighted non-contrast imaging (TWILITE)^{9,11} is used to accurately depict acute RFA injury that is of sufficient thermal dose to lead to tissue necrosis. Typically, RFA at each location requires 60–90 s, and a typical left-atrial clinical study may include 30 ablations.

One of the largest issues with MR-guided EP is the lack of sufficient imaging Signal-to-Noise Ratio (SNR) for fast

ablation monitoring. Conventional cardiac and spine surface arrays require long acquisition times (12–15 min) for the LGE and TWILITE sequences^{9,11} to obtain sufficient SNR at the $\sim 1 \times 1 \times 1 \text{ mm}^3$ spatial resolution required to image lesions in the thin atrial walls, or detect small electrically-conductive channels within dense ventricular scar after myocardial infarction (MI).^{8,12} Additionally, during such long scans, patient breathing and heart-rate can drift, further increasing the scan time. Long MRI scan times can greatly extend the duration of MRI-guided interventions, increasing patient risk due to longer anesthesia times.

Intracardiac Echo (ICE) has improved the monitoring of EP procedures, since the invasive ultrasound probe, inserted in tandem with a variety of interventional devices, provides far better visualization at key stages of the X-ray guided EP procedure, such as during the puncturing of the trans-septal hole between the right and left atria,^{13,14} or while mapping structures not visualized by fluoroscopy. Similarly, an intracardiac MRI coil might be useful to improve MRI-guided EP when improved spatial resolution or faster acquisition imaging is desired.

In MRI studies of other diseases, it was established that locally-placed coils, such as the endorectal prostate coil^{15,16} and the esophageal coil,¹⁷ greatly improve imaging of small anatomy or pathology, if the coil is brought sufficiently close to the target organ.¹⁸

MRI coils for high-resolution cardiovascular imaging were previously studied. MRI coils were developed for placement in the esophagus¹⁷ and in the coronary arteries.^{19,20} Other designs included expandable MRI coils placed inside an inflatable balloon.^{21,22} Bottomley's group constructed intravascular coils for use at 3T and 7T.^{23,24}

Endovascular imaging-coils must be placed on long ($\geq 900 \text{ mm}$) and small (2–6 mm) diameter catheter shafts, so that they can be advanced to their targets through the

vascular tree. When multiple sensors are required, the MRI signals originating from the distal end are carried on small, 50 Ohm characteristic impedance dielectric-filled, 42–50 American Wire Gage (AWG), (0.063–0.025 mm inner-conductor-diameter (ID)) micro-coaxial cables to the proximal end. These are far more lossy than larger coaxial cables. Typical 1.5T flexible (non-rigid) micro-coax insertion-loss: 50 AWG (0.063 mm OD, 0.025 mm ID); 6.5 dBm⁻¹, 46 AWG (0.13 mm OD, 0.041 mm ID); 3.3 dBm⁻¹, 42 AWG (0.29 mm OD, 0.063 mm ID); 1.6 dBm⁻¹. 3T insertion-losses: 30%–40% higher than 1.5T.^{25–28} As a result, the SNR at the proximal catheter-end is far lower than the SNR received at the distal end, reducing the achievable image quality.

We aimed to develop an intracardiac MRI imaging (ICMR) guiding-sheath, navigated into the heart in tandem with EP ablation catheters, thus performing navigation similarly to that performed with deflectable guiding-sheaths (eg Abbott Labs Agilis, Minnetonka, MN) as well as providing faster imaging of RF ablation.

The first requirement for utilizing ICMRI (I) was to be able to navigate through the vascular system, restricting the catheter outer-diameter during the *vascular navigation phase*. (II) Effectively navigating (pushing, rotating, torquing) thin sheaths called for a high mechanical-strength, which typically requires use of metallic-braided shafts. (III) Another requirement is to allow an MR-conditional deflectable EP ablation-catheter's tip²⁹ to protrude sufficiently in front of the sheath, so it can be deflected and moved between chamber-surface points, which also insures the imaging-coil is not damaged by the EP catheter tip during ablation. (IV) The principal utilization target was determined to be the left atrium (LA), whose central diameter is 40–70 mm,^{30–32} setting the imaging-coil's desired Field of View (FOV). (V) The central LA diameter restricts the maximal size of the imaging-coil *when deployed for imaging*, which (VI) has implications on the maximal SNR gain, relative to surface coils (i.e. the spine-array and body-array coils) used in cardiac imaging. (VII) The ICMRI guiding-sheath needed to be actively-tracked during navigation in the MRI and, possibly also outside the MRI, which would allow partial procedure performance outside the MR scanner. (VIII) To perform actively-tracked arrhythmia ablation procedures, a navigational workstation is needed.

The ICMRI 3T and 1.5T prototypes were constructed by Abbott Laboratories (Minnetonka, MN). We tested ICMRI in ex-vivo hearts to determine whether it delivered imaging performance in line with specifications and then in gel phantoms to determine MRI safety during high Specific Absorption Rate (SAR) MRI sequences. We then evaluated ICMRI performance during swine interventions, where we tested actively-tracked navigation together with EP

catheters, and imaging with TWILITE sequences during RFA. Since the 3T ICMRI was developed (2015–2017) before the 1.5T version (2018–2020), slightly inferior catheters were used at 3T. The improvements were improved tip deflection and the robustness of imaging-coil expansion and folding. Presentations on older ICMRI versions are included.^{33–36}

2 | METHODS

2.1 | ICMRI-catheter detailed specifications in response to requirements

(I) To allow effective navigation through the vascular system in tandem with an internal 2.5 mm OD EP catheter, but permit use of a larger imaging-coil during the imaging phase, we defined the maximal catheter diameter during navigation to be 7 mm and required use of an expandable imaging-coil. (II) To allow use of a device with a long (>quarter wavelength) metallic shaft, we decided to add miniature resonant RF traps (MBaluns) to the shafts, in order to substantially reduce radio-frequency-(rf)-induced heating.³⁷ We choose the common-mode attenuation at the most distal MBalun to be –30 dB, which set the distance between successive MBaluns.³⁷ (III) To allow EP catheter deflection in the LA, we decided that the catheter's tip²⁹ should protrude 30–50 mm in front of the tip of ICMRI's shaft. (IV) The adult LA's minimum central diameter (39–45 mm) restricted the expanded imaging-coil diameter to 35 mm, which (V) restricted the effective imaging-coil's Field of View (FOV) to 50–60 mm in each spatial direction. (VI) We desired to perform imaging at ~50% of the time required using current surface coils, which required a minimum SNR boost of 400%, over the central LA, a 4 × 4 × 4–6 cm³ FOV. This FOV allows covering large regions of the LA chamber (eg during surface mapping or ablation) while leaving a stationary ICMRI, reducing procedure complexity. Also, to preserve the achieved SNR gain at the proximal end of the ICMRI catheter, we decided to place a tuned, matched and decoupled LNA circuit close to the imaging-coil as previously suggested.²⁶ Due to the catheter size, this required use of miniature die components. (VII) To actively-track catheter navigation, we used a MR-Tracking (MRT) sequence with multiple-directional Phase Field Dithering (PFD), reducing location-errors due to coupling to neighboring metallic structures.³⁸ Due to MRT-coil placement on metallic surfaces, we employed previously-developed flexible printed circuit loop-coils.^{39,40} Also, to allow ICMRI utilization as a sheath for active-navigation both inside and outside the MRI scanner, as demonstrated previously,⁴¹ two impedance-tracking ring electrodes^{41,42} (Abbott

Ensite-NavX) were placed on the distal shaft. (VIII) To perform arrhythmia-ablation procedures, a⁴³ navigational workstation was required which displays data from various sources, such as MRI images and electroanatomic maps, and overlays these with the current catheters' location and shape, based on MR-Tracking and impedance-tracking data streamed to the station.

2.2 | The metallic-braided ICMRI guiding sheath

Details of the electrical circuits, components and their manufacturers are included in Supporting Information Figure S1.

2.2.1 | The ICMRI shaft

The ICMRI shaft (Figure 1A) consisted of a 6 cm long distal region that contained the imaging and MRT coils, a 1 m long shaft, and a 10 cm long proximal handle (Figure 1).

Its 18-French (6 mm) OD metallic-braided tin/copper sheath had 6 minor lumens for passage of five 44 AWG (0.051 mm ID, 0.23 mm OD) micro-coaxial cables for the imaging and MRT coils, two copper 48 AWG (0.0305 mm OD) single-ended cables for the impedance-tracking electrodes, as well as for passage of the nitinol pull-wire which deflected the distal tip. These surrounded an 8.5 Fr (2.8 mm) diameter open lumen, allowing insertion of an EP ablation catheter.

To reduce the MRI's body-coil inducing common-mode currents causing temperature increases (heating) in ICMRI's metallic braided shaft, as well as in the signal-transmission cables running within, 10 MBaluns³⁷ were mounted at 85 mm increments along the shaft, starting 10 mm from the distal end. The MBaluns consisted of 38-AWG (0.102 mm OD) magnet-wire windings (3T: 5 mm long MBalun, 15 windings, Electromagnetic (EM) simulation calculated: 230 nH effective (radial and circumferential components only) inductance, -35 dB Common Mode (CM) attenuation 3 mm proximal to the distal MBalun. 1.5T: 10 mm long MBalun, 27 windings, EM simulation calculated: 470 nH effective inductance, -28 dB CM

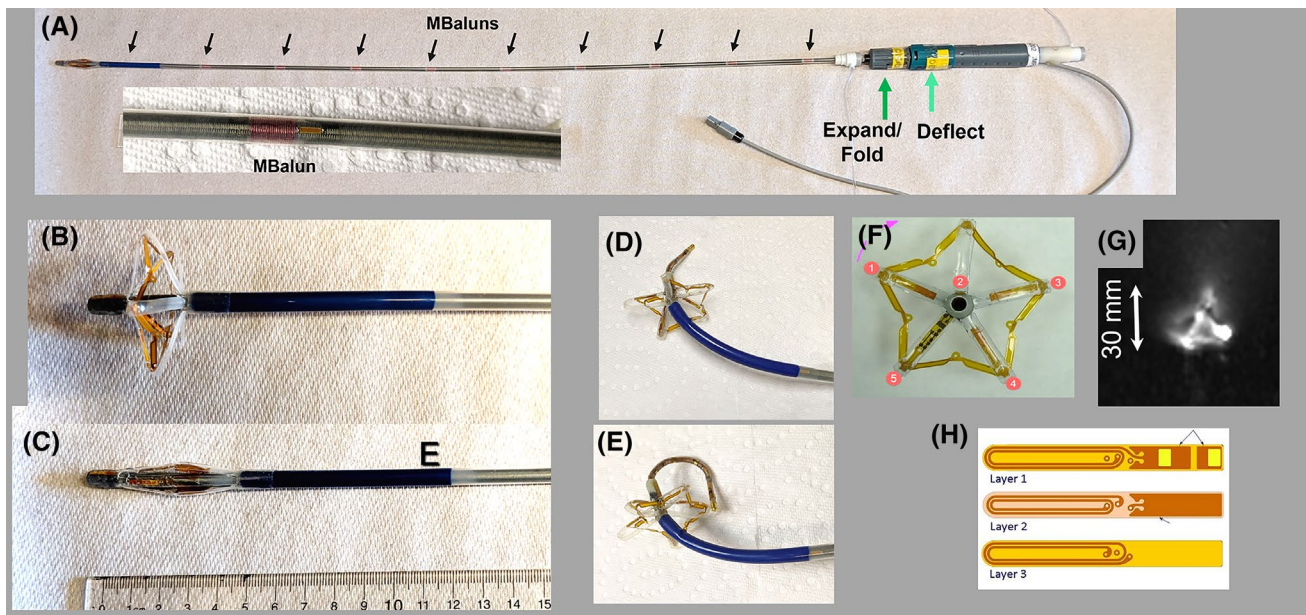


FIGURE 1 1.5T ICMRI guiding sheath. (A) The complete metallic-braided catheter showing locations of the heat-ameliorating MBaluns along the shaft as well as the two levers, which activate the tip deflection (dark green) and imaging-coil expansion or contraction (light green). Expanded view of an MBalun mounted on the braid shows the solenoidal wires and the FPC capacitor. (B) Distal end of ICMRI, showing the imaging-coil expanded (35 mm ID) during imaging or (C) folded (6 mm OD) during vascular access. (D and E) Pull-wire deflected distal ends of ICMRI, along with the protruding distal-tip of a deflected EP catheter, demonstrating the anatomical-access capabilities permitted by manipulating both devices. (F) On-face view of the expanded imaging-coil and supporting struts, showing the location of the four MRT coils¹⁻⁴ and the protected pre-amplifier electronics of the imaging-coil.⁵ (G) MR Image of expanded imaging-coil shows the tetrahedron shape of the four MRT coils, which allow accurate tip localization. (H) Construct of the 1.5T three-layer loop-design MRT FPC board (length 14 mm, width 1.2 mm, thickness 0.25 mm). The MRT coil contains both the antenna and embedded parallel and series T&M capacitors. The 3T MRT coils were of similar construct but contained only two layers (to reduce inductance) and utilized lower-value T&M embedded capacitors

attenuation 3 mm proximal to the distal MBalun), wound at a normalized pitch ($= \frac{\text{distance between windings}}{\text{wire-diameter}}$) of 2 around a 0.3 mm thick insulator which was placed above the braid, with one end of the wire soldered to the braid and the second end connected to the braid via a 0.2 mm thick Flexible printed circuit (FPC) 9 pF embedded capacitor.

2.2.2 | The distal expandable MR-imaging and MR-tracking coils

The distal catheter section (Figure 1B,C) is 6 cm long when folded for vascular access, and constructed of Pebax 7233 elastomer. It was constructed of a tube cut into 5 equal leaflets (every 72 degrees), which expanded when the leaflets were pushed and shortened, using force exerted by a 0.5 mm thick cylindrical shaft inside the braided shaft, whose motion was driven by a rotary lever on the catheter handle. With the handle fully rotated, the section shortened to 3 cm length and expanded to 35 mm diameter.

The MRT coils were constructed (Figure 1H) of multi-layer FPC boards with two loops per layer. Two-layer 3T coils and three-layer 1.5T coils were used. Embedded parallel and series capacitors, constructed of rectangular copper films surrounding a 13 μm dielectric film (M C1012 Embedded Capacitance Material), were used to tune and match (T&M) the MRT coils on the FPC. 3T MRT-coil dimensions; (Length, Width, Thickness = 8 mm, 1.2 mm, 0.25 mm); capacitors: 8 pF series, 12 pF parallel capacitors. 1.5T coil dimensions; (Length, Width, Thickness = 8 mm, 1.6 mm, 0.27 mm); capacitors: 22 pF series, 82 pF parallel.

When ICMRI's imaging-coil was expanded, the MRT coils attained a tetrahedron shape (Figure 1D) with 17 mm diagonals, with three leaflet-mounted micro-coils centered 20 mm from the proximal leaflet end, and the fourth micro-coil 5 mm from the distal tip. The rf signals were conducted up the shaft on 44 AWG micro-coaxial cables.

Two impedance-tracking electrodes were placed on the non-expanding shaft at 0.5 mm (directly above the MR-Tracking coil) and 90 mm distances from the tip.

ICMRI's imaging-coil had a 5-vertices "star"-shaped design, constructed of FPC (Figure 1B). The coil was made of two loops (Figure 2C, Supporting Information Figure S1A), that also included five (3T: 25 pF, 1.5T: 50 pF) embedded series capacitors to reduce phase dispersion. Embedded capacitors were used, since they did not increase the printed-circuit's thickness. The embedded capacitors also had a larger surface area than multilayer ceramic capacitors, which contributed to a lower resistance at rf frequencies, and increased the unloaded Q of the coil to ~ 500 .

The elongated imaging-coil stem (Figure 2B,C) contained electrical-circuits and connections to the micro-coaxial cable, which conducted the Larmor radio-frequency signal up the shaft. This section contained parallel (3T: 68 pF, 1.5T: 27 pF) and series (3T: 33 pF, 1.5T: 10–12 pF) T&M embedded capacitors. The capacitors were followed by a protected amplification unit (Figure 2A, black enclosure, Figure 2B), composed of two antiparallel pin-diode wafers (protecting the low-noise-figure (0.57–0.65 dB) pre-amplifier (LNA) wafer from high-power input during rf transmission. The LNA received 30–60 mA, 3.0V DC from 3.7V MR-conditional batteries. When powered, the pre-amplifier drew ~ 0.3 Watts, which initially heated the pre-amplifier's enclosure, but heating was reduced to $\sim 2^\circ\text{C}$ in saline-solution by attaching the pre-amplifier base to large surface-area thermally-conductive pads on the FPC and ensuring the proximal micro-coax (eg at the guiding-sheath handle) received only 3.0V DC, achieved by placing a 12 Ohm resistor at the battery output. The pin-diode and LNA wafers were enclosed in an epoxy box (Length, Width, Thickness = 1.5, 1.5, 0.75 mm) to prevent water ingress, and prevent the stem from bending.

When powered, the LNA increased the measured rf power of the received MR signals by 27 ± 2 dB at 1.5T and 3T, relative to a tuned and matched coil without a pre-amplifier. This improved the imaging-coil SNR at the proximal catheter end by 3–4 dB,²⁶ after the signal was propagated up the 1-meter shaft, reducing the detrimental effect of the lossy micro-coaxial cable.

2.2.3 | System electronics box

To enhance the tracking-coil and imaging-coil signals by correcting for phase changes resulting from the 1 m long coaxial transmission, a systems electronics box was placed between the ICMRI catheter and the 8-channel receiver (Figure 3A, Supporting information Figure S1C). It contained a T&M pi (π) circuit for each MR-Tracking channel, consisting of two parallel adjustable capacitors surrounding a series adjustable inductor. Anti-parallel pin-diodes and a 1.5 kV 901 pF DC blocking capacitor were also placed on the tracking channels (Supporting information Figure S1C) to decouple the tracking coils and to prevent DC current from flowing down the catheter, complying with IEC 60601⁴⁴ high voltage and DC leakage-current regulations.

In addition, a custom MRI-conditional Bias-Tee (B-T) circuit (Figure 3C, Supplementary Figure B) was connected to the imaging-coil's receiver-channel in the electronics-box. The B-T circuit allowed 3.0 Volt 33–60 mA DC current from the battery to propagate down the catheter shaft and power the LNA and also

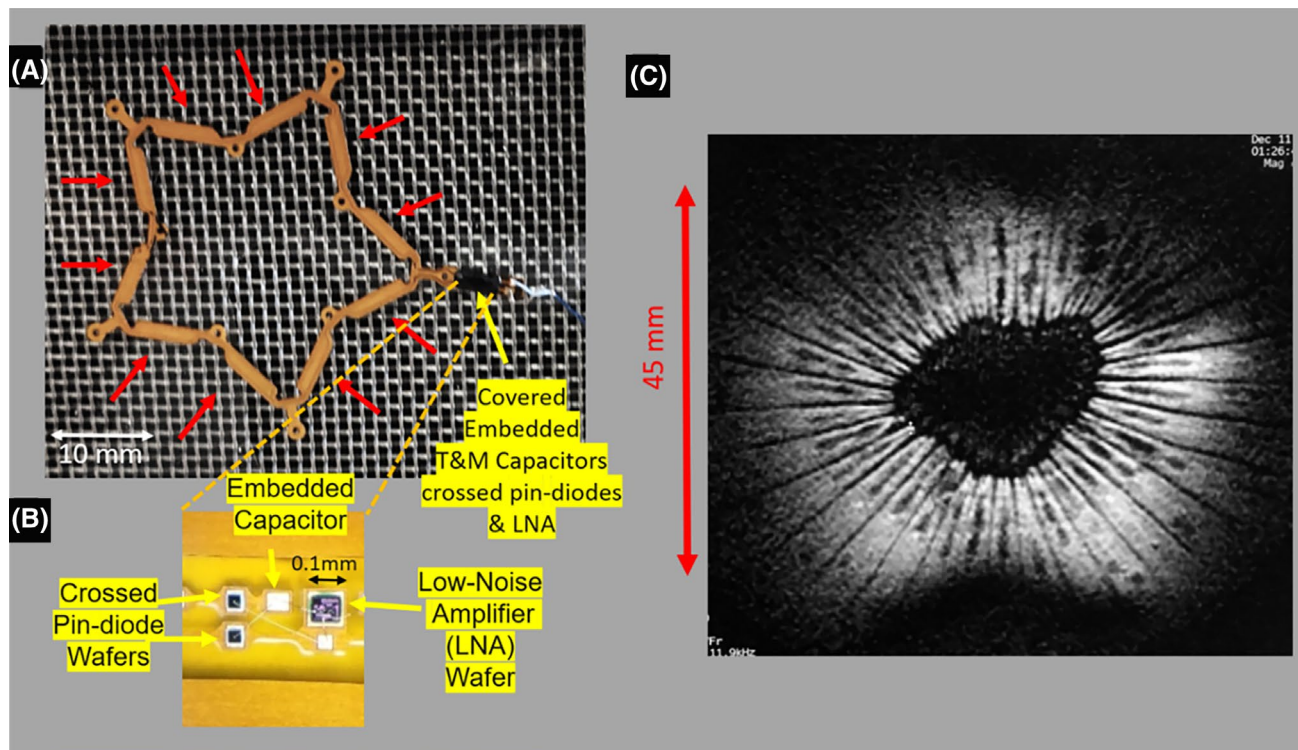


FIGURE 2 ICMRI imaging-coil. (A) 3T FPC pentagon-shaped coil with thin-film embedded series capacitors on its shaft (red arrows). The 2-winding coil circuit also includes an integrated front-end (Yellow arrow) placed on the connecting stem, which includes T&M embedded capacitors, anti-parallel pin diodes for high-signal amplifier protection and a low-noise pre-amplifier, all encased within the (black) epoxy waterproof box. The 1.5T coil is similarly built, except for different capacitors on the pentagon and on the stem. (B) Enlarged view of the antiparallel pin-diode wafers and low-noise amplifier wafer taken with a microscope during component wire-bonding, and before encasement in the epoxy box. Circuit detail is shown in Supporting information Figure S1A. (C) GRE image (parameters: TR/TE/ θ = 3.3 ms/1.2 ms/30°, 4.5 × 4.5 cm² FOV, 225 × 225, 2 mm slice-width, 0.2 × 0.2 × 2 mm³, 3 s acquisition) of a sliced Kiwi fruit 20 mm away from the coil demonstrates the coil's effective FOV when it is open

prevented DC current from going upstream towards the 8-channel receiver. The B-T was composed of a parallel 0.1 μ F capacitor to ground, followed by two series 2.2 μ H air-core inductors. The B-T circuit was powered by two parallel MRI-conditional rechargeable lithium-ion 3.7 V batteries. Voltage from the batteries then passed through the B-T circuit. After the inductors, the circuit split into two parts, which were connected to the rf coax leading from the imaging-coil to the receiver; one end toward the imaging-coil and the other end towards the 8-channel receiver. A series 1.5 kV capacitor was placed in series along the 8-channel receiver direction to prevent DC from flowing to the receiver. The B-T's parallel 0.1 μ F capacitor prevented AC current from flowing from the battery to the imaging-coil transmission-line during switching OFF/ON of the battery, while the B-T's series inductors prevented rf from flowing towards the battery. Further upstream, after going through a T&M π circuit, the imaging-coil signal went to a dedicated channel of a custom 8-channel receiver, with separate custom receivers utilized for the 1.5 and 3T ICMRI prototypes.

2.2.4 | ICMRI proximal handle

At the catheter's proximal end was a handle, with two rotatable controls, which enabled (a) the expansion and closure of the distal star coil, as well as bi-directional deflection of the distal end by 90 degrees (Figure 1A). A 14-pin quick-disconnect Redel connector (Lemo, Switzerland) connected the signals from the four MRT coils and the imaging-coil to the custom 8-channel MRI receiver. A separate connector carried the two Impedance-tracking signals out towards the Abbott Labs Ensite-Velocity system. A hemostatic valve on the catheter handle prevented blood in the guiding-sheath's lumen from leaking outwards.

2.2.5 | MRI-compatible 3T and 1.5T actively-tracked deflectable ablation catheters

Abbott Labs constructed 7.5-French (2.48 mm) OD metallic-braided actively-tracked deflectable EP catheters with MBaluns for this study (Figure 2D,E). These catheters are described in detail elsewhere.^{29,37} Each catheter had a

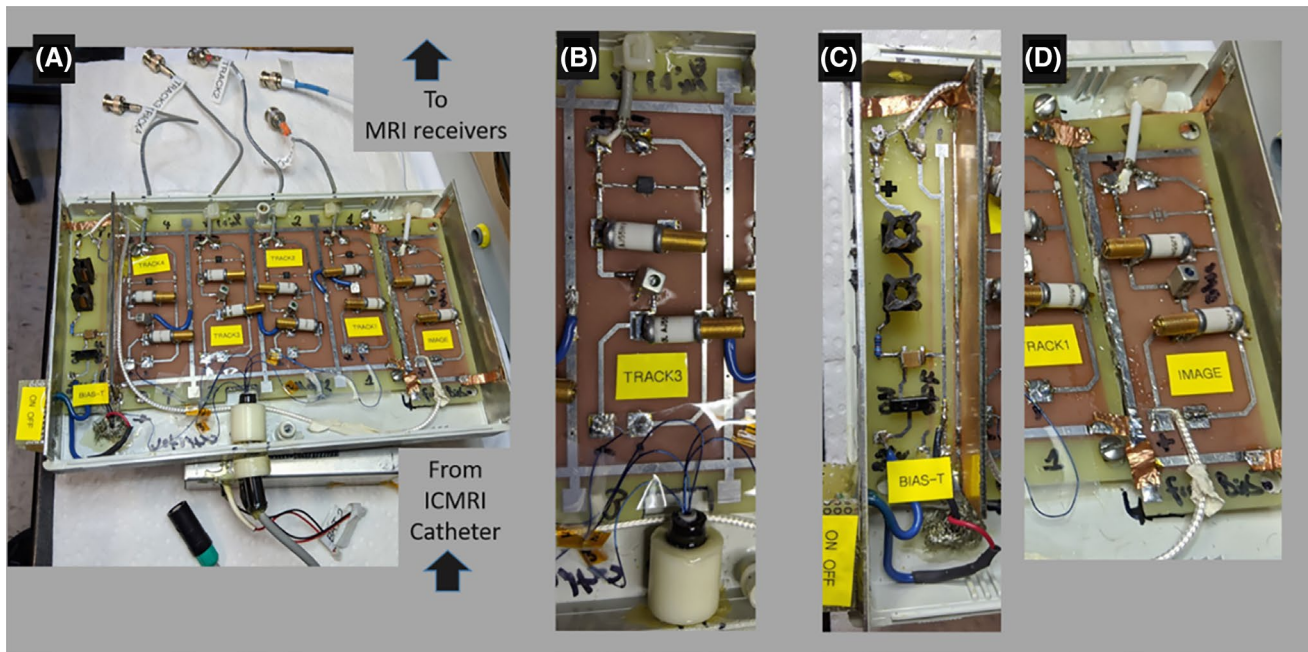


FIGURE 3 System electronics box. (A) Electronics box connects to ICMRI and conditions the signals in the four tracking channels (Track1-4) and in the imaging channel (Image). (B) Enlarged Imaging channel, showing the π circuit T&M which compensates for the phase shifts produced by the 1 m length microcoax, along with a passive decoupling (antiparallel pin diodes) circuit and 1 KV (0.1 μ F) capacitive blocking circuits that protect the patient from DC leakage currents and High AC voltages. (C) The LNA at the ICMRI tip is powered by two parallel rechargeable MRI-conditional Lithium-Polymer batteries which provide 3.7-4.0V DC (not shown), although only 3.0V reach the LNA due to losses in a resistor and in the micro-coaxial cable. The DC current passes through an MRI-conditional Bias-T circuit, which prevents RF noise from entering from the battery, and also prevents DC current from going upstream to the MRI receiver. The B-T was composed of a parallel 0.1 μ F 1 KV capacitor to ground, followed by two series 2.2 μ H air-core inductors. At the point designated with a black \pm sign, the DC signal is combined with the amplified raw MRI signals from the LNA's output. (D) The imaging channel receives the imaging-coil's amplified signal from (C) and also has a π circuit to T&M the amplified signal coming from the ICMRI tip, as well as a 1 kV blocking capacitor to protect the patient. Circuit diagrams are included in the Supporting information Figure S1.

gold-plated copper 4-mm ablation tip and four 3-mm width ring electrodes, at electrode-center distances from the tip; 0 cm, 0.8 cm, 5.0 cm, 7.5 cm, 9.5 cm. The electrodes served for recording intracardiac ECG traces and for MR-conditional impedance-tracking.^{41,45} The tip electrode was also employed for RFA delivery. The EP catheters also included four MRT micro-coils, at center distances from the tip; 0.6 cm, 1.9 cm, 3.6 cm, 5.5 cm. The EP-catheter's handle included a deflection lever, and a Redel connector that transmitted the tracking signals. A "Y"-shaped connector, connected to the Redel, split signals from the catheter between the impedance-tracking and the MR-Tracking receivers. The MR-tracking receiver-path proceeded to an electronics box with a T&M circuit like ICMRI's electronic box. The MR-tracking signals were then connected, via half-wavelength-length coaxial cables, to a custom 8-channel MRI-receiver.

2.2.6 | 3D slicer MR tracked navigation

A dedicated application for MR-Tracked cardiac navigation was developed on the NIH-funded open-source

medical image computing software, 3D Slicer⁴³ with a custom plug-in module implemented using the Python language (<https://github.com/mrtracking/Mrtracking>). It allowed navigation on sets of roadmap MR images using built-in visualization algorithms, including (a) 2D slice reformatting, (b) GPU-accelerated volume rendering, and (c) 3D surface rendering (Figure 6). For surface rendering, 3D Slicer offered manual or semi-automatic tools to segment the anatomical structures based on native or contrast-enhanced 3D MRI images, and used the marching-cube algorithm⁴⁶ to convert the segmented data to a surface polygon model.

MR-Tracked locations on the EP catheter and on ICMRI, acquired simultaneously at 16 fps from ICMRI and the EP catheters' MRT coils, were sent directly from the Siemens MR scanner's reconstruction engine to 3D Slicer through the 1000-Base T Ethernet using the OpenIGTLink network communication protocol.⁴⁷ 3D Slicer estimated the shape of the catheter by interpolating the tracked locations from each device using spline interpolation and generated a surface model of the catheter-shaft of the EP catheter's and ICMRI's distal ends. The model was then

overlayed onto the roadmap MRI rendered by any of the visualization algorithms listed above. Supporting information VideoS1 shows joint MRI-Tracked navigation of the ICMRI catheter and a protruding deflectable EP catheter inside a human-sized LA model (Abbott laboratories) filled with saline solution, which was placed within a human-sized torso phantom, showing access to several PV ostia and the LA roof.

2.2.7 | ICMRI testing at 3T and 1.5T in ex-vivo swine hearts and in-vivo swine

All animal experiments were performed under approved Brigham and Women's Hospital (3T) and Johns Hopkins Hospital (1.5T) IACUC protocols. ICMRI testing was performed at 3T on a Siemens Skyra (software version VD13) and at 1.5T on a Siemens Aera (software version VE11C).

2.2.8 | ICMRI tissue heating in ASTM F2182-19e2 gel phantom

A disconnected ICMRI guiding-sheath was placed in a gel phantom with the tip located 15 cm off-center along the x , y and z , locations where maximal electric field induction from the body coil was expected.⁴⁸ Further details are presented elsewhere.³⁷ Fiberoptic probes were placed at locations near the tip where maximum heating was expected, as well as at a reference location far from the device. A 4 Watt/kg Specific Absorption Rate (SAR) SSFP sequence was run for 15 min. Separate runs were performed at both 1.5 and 3T, with the imaging-coil folded, as occurs during navigation, and with the coil expanded, as occurs during imaging.

2.2.9 | Electromagnetic simulated, ex-vivo and in-vivo heart imaging-coil SNR and effective FOV estimation

Electromagnetic simulation of the imaging-coil performance was performed at 63.8 MHz using HFSS 2021 R2 package (Ansys, Canonsburg, Pennsylvania) by placing the imaging-coil in a cylinder of simulated blood, with the blood conductivity and dielectric constant values selected from <https://itis.swiss/virtual-population/tissue-properties/database/dielectric-properties/>. Details are in Supporting Information Figure S2.

ICMRI testing was first performed in an excised swine heart. The goal was to determine the effective FOV of the expanded imaging-coil in-situ, as well as to determine the SNR benefit of the ICMRI imaging-coil relative to

the scanner's surface arrays. The excised heart, placed in a large plastic container filled with normal-conductivity saline solution, was distanced from the spine array by 20 cm and 15 cm from the body array, representing a patient torso 35 cm long in the Anterior-Posterior direction. The ICMRI imaging-coil was inserted into the Left Atrium of the excised heart, and images acquired using both ICMRI and the scanner's cardiac and spine surface arrays. T2-weighted scans were used; parameters: Fast Spin Echo, TR/TE/ θ = 2000 ms/90 ms/180°, ETL = 14, 128 × 256, FOV = 30 × 30, slice-width (sw) = 4 mm.

A second test was performed in a large anesthetized normal swine (weight 50 kg). A conventional (non-MRI-conditional) trans-septal needle was used in the X-ray lab, together with a conventional 0.035" metallic guidewire, to puncture the atrial septum and gain access to the left atrium. This test was performed before MRI-conditional needles and guidewires were developed.⁴⁹ The ICMRI guiding-sheath was introduced via a 20 Fr 30 cm long introducer (Abbott labs Hemostatis) into the femoral vein, and then navigated in the X-ray lab to the right atrium, there after to the atrial septal wall, and then through the previously created hole into the left atrium. The ICMRI handle was sutured to the animal's skin, and the animal was transported to the MRI scanner, where ECG sensors were added, and the spine and body arrays mounted on the animal. 2D ECG retrospectively-gated Gradient Recalled Echo (GRE) images were acquired along the axial, coronal, and sagittal directions, centered on the heart (parameters: 36 encodes/RR at end-systole, TR/TE/ θ = 15 ms/3 ms/15°, 128 × 256, FOV = 35 × 35, sw = 10 mm).

Coil Coverage (3D FOV) was estimated by measuring the locations of the 70% amplitude drop-offs, relative to the peak amplitude. The apparent coil SNR was measured as the mean signal-intensity in a 5 × 5 × 5 mm³ voxel ROI at the center of illumination, divided by the Standard Deviation (SD) of the signal-intensity in the animal lungs or in the air around the body (ie in noise). The SNR boost in percent provided by the ICMRI imaging-coil was estimated by dividing the mean signal-intensity over a 3 × 3 × 3 cm³ FOV by the combined signal-intensity of all the surface-coil elements at that location, as determined by performing image reconstructions that provided the signal-intensity of each array element.

2.2.10 | Navigation in swine using ICMRI and EP catheters, with RFA monitoring in the RV and LA

5 anesthetized normal (30–50 kg weight) swine at 3T and 5 at 1.5T were used. 20 Fr 30 cm long introducers were placed into the femoral veins. Under X-ray fluoroscopy

guidance, the ICMRI guiding-sheath was introduced into the femoral vein, and then navigated together with a protruding EP catheter in the X-ray lab to the Right Atrium, and thereafter to the atrial septal wall. A conventional metallic trans-septal needle was used to perforate the atrial septum, and the EP catheter was then advanced in the LA. With left-atrial access assured, ICMRI and the EP catheter were withdrawn to the femoral arteries, sutured to the skin, and the animals transported to the MRI scanner.

At the MRI scanner, the swine were connected to MRI-conditional Invivo Precision (Gainesville, FL) physiological monitoring (CO_2 , SPO_2 , ECG) and placed on MR-conditional respirators. Four-lead ECG pads and the body-array coil were placed on the swine chest and they were inserted in the MRI bore. A balanced SSFP cardiac-gated axial scan (parameters: $T_R/T_E/\theta = 4 \text{ ms}/1.5 \text{ ms}/30^\circ$, $35 \times 35 \text{ cm}$ FOV, 320×320 matrix, 2 mm slice-width, 2 averages, no interslice gap) was performed during 3 forced breath-holds, spanning from the femoral veins to above the aortic arch. The images were then transferred to the 3D Slicer workstation, for use as navigational roadmaps for the procedure.

An MRT pulse-sequence⁴⁰ (parameters: $T_R/T_E/\theta = 2.2 \text{ ms}/1.1 \text{ ms}/8^\circ$, 35 cm FOV, 384 pixels, 3 PFD, 3 avg, 12 frames-per-second, $0.9 \times 0.9 \times 0.9 \text{ mm}^3$ resolution) was used to actively navigate the ICMRI guiding-sheath, using its MRT coils and deflectable tip, up the vena cava to the Right Atrium or Right Ventricle. In experiments where left-heart access was performed, an EP catheter was then advanced through ICMRI to the trans-septal hole and pushed into the left atrium, thereafter followed by ICMRI's insertion through the atrial septum.

Once the target location was reached, ICMRI's imaging-coil was expanded at approximately 30 mm from the cardiac-chamber wall, with the EP catheter protruding 30–60 mm outwards. Imaging was performed using ICMRI's imaging-coil as well as the body and spine surface coils in a combined array, using 3D GRE (parameters: Navigator-echo-respiratory triggering, 1RR systolic gating $T_R/T_E/\theta = 650\text{--}900 \text{ ms}/1.2 \text{ ms}/25^\circ$, 488×512 , FOV = $20 \times 20 \text{ cm}^2$, sw = 1.0 mm BW = 252 Hz/pxl, 1 avg, 40 slices/scan, 7:20±:0:30 min acquisition time) or 3D TWILITE (parameters: Navigator-echo-respiratory triggering, 2RR systolic gating, $T_I/T_R/T_E/\theta = 500 \text{ ms}/1300\text{--}1800 \text{ ms}/1.2 \text{ ms}/25^\circ$, $35 \times 35 \text{ cm}$ FOV, 320×320 matrix, 1 mm slice-width, 1 average, 50 slices/scan, 13:30 ± 1:00 min acquisition time) sequences. ICMRI imaging alone was performed to accelerate acquisition following RFA using the above sequences, excluding the following parameter changes ($14 \times 14 \text{ cm}$ FOV, 144×144 matrix, 3D GRE-3:30 ± 0:30 min acquisition time, TWILITE-5:30 ± 1:00 min acquisition time).

RFA was delivered from an RF ablation generator (Ampere, Abbott Labs) placed within the MRI scanner

room in an rf-shielded cabinet, with Radio-Frequency-Interference filtered connections to the MR-conditional EP catheters. 20 Watt were delivered for 90 s to each lesion, while monitoring the surface impedance between the EP catheter and the wall. While ablating, water irrigation was continuously delivered to the EP catheter tip by an irrigation pump (Coolpoint, Abbott Labs), found in the rf-shielded cabinet, to prevent excessive catheter-tip heating.

3 | RESULTS

3.1 | ICMRI tip temperature increases during 4 Watt/kg SAR imaging in a gel phantom

Results for the 1.5T thermal tests for a disconnected ICMRI are shown in Figure 4A,B, for situations when the imaging-coil is folded, as utilized during vascular navigation, and for when it is expanded, as required for imaging. In these tests, the guiding-sheath was not electrically connected and the LNA was not powered. When folded, the maximum temperature increase ($1.6 \pm 0.1^\circ\text{C}$) was observed on the surface of the LNA (denoted IC), which is only slightly above ASTM/IEC/FDA limits (1.5°C). When the coil was fully expanded, ASTM limits were exceeded after 3 min, and only in areas distal to the first MBalun on the shaft. Since the heat sinks placed on the FPC boards are not effective in the gel phantom, we expected to meet ASTM limits when working in convective blood vessels. In later swine in-vivo experiments, we never observed blood coagulation around the imaging-coil, which is expected if substantial heating occurs.

3T heating experiments (Figure 4C,D) were performed in a disconnected ICMRI and resulted in folded-coil: $1.8 \pm 0.1^\circ\text{C}$ and expanded-coil: $13 \pm 0.1^\circ\text{C}$ heating, with the largest heating observed on the LNA enclosure.

We performed a 3T heating test in a saline solution with ICMRI electrically connected to the electronics box and the LNA powered ON. This resulted in folded coil: $1.4 \pm 0.1^\circ\text{C}$ and expanded coil: $1.8 \pm 0.1^\circ\text{C}$ heating on the LNA enclosure. This suggests that the larger heating of the expanded imaging-coil was primarily because of the higher expanded-coil inductance.

3.2 | Electromagnetic simulated and measured imaging-coil SNR and Coverage

Supporting Information Figure S2, parts B-F shows Electromagnetic simulated results for the ICMRI imaging-coil in simulated blood at 1.5T. The expanded coil has a

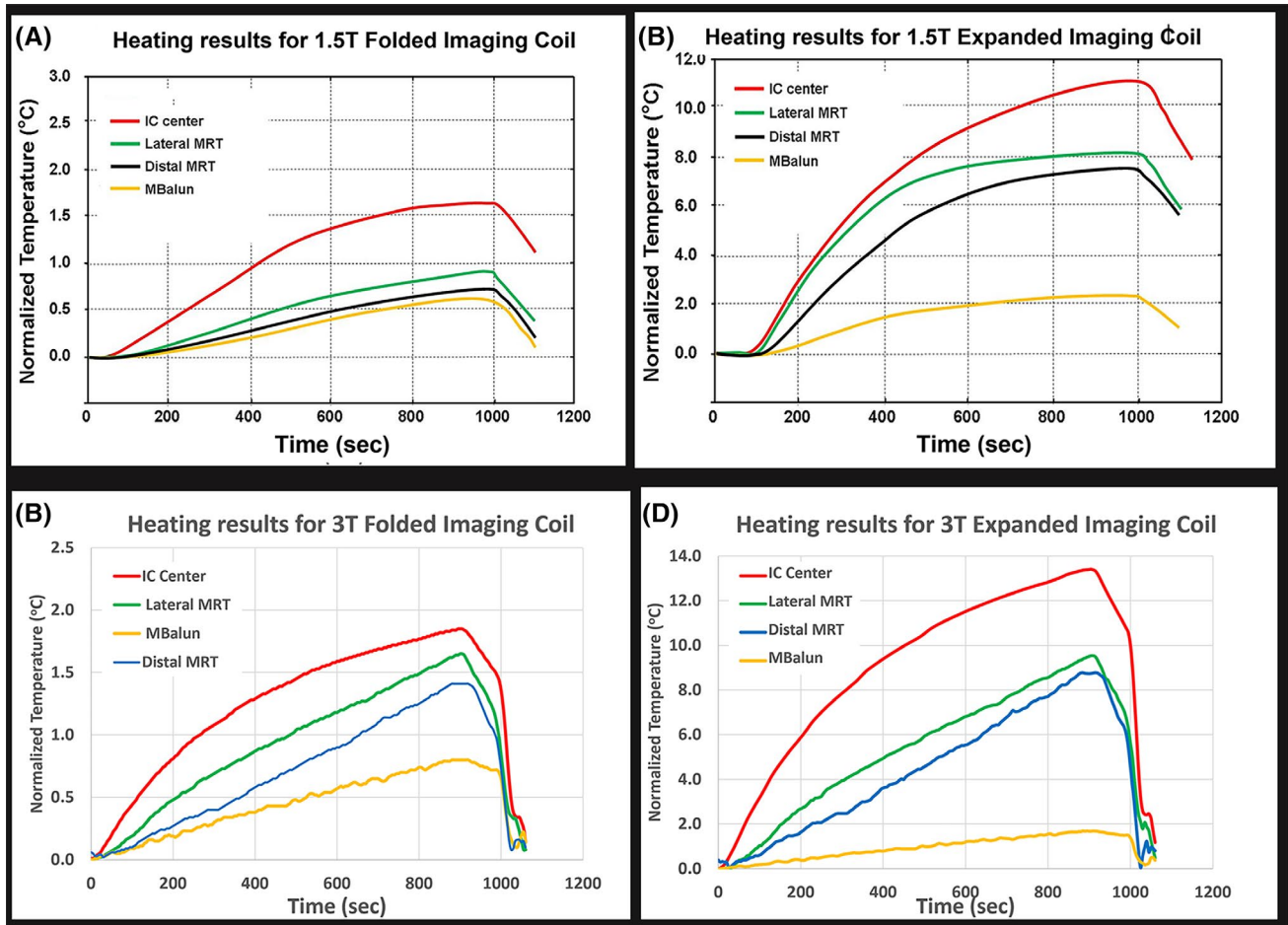


FIGURE 4 1.5T (A, B) and 3T (C, D) heating tests performed on a disconnected ICMRI in a non-convective ASTM gel phantom during 15-min continuous 4 Watt/kg SAR imaging with the LNA not powered. (A, C) 1.5T and 3T folded (6 mm OD) imaging-coil, as used during navigation. (B, D) 1.5T and 3T expanded (35 mm OD) imaging-coil, as used during imaging. IC denotes the epoxy box which encloses the LNA and its protecting pin-diodes, which is connected to a heat sink on the FPC, which is not effective in the gel phantom. During navigation with the coil folded, ICMRI slightly exceeded ASTM/IEC limits of 1.5°C maximum heating at 1.5 and 3T. With the imaging-coil expanded, portions of the 1.5 and 3T ICMRI imaging-coil, at points distal to the MBalun, exceeded 1.5°C after only approximately 80 s, rising to 12°C and 13.2°C, respectively, after 15 min

pentagram-shaped in-plane radiation pattern, with the maximal B_1 - (Figure S2, B) observed in the center plane close to the coil windings, with a 26% drop in amplitude in a 5 mm-diameter region at the center. In planes perpendicular to the coil plane, the amplitude (Figure S2, D-F) drops by 50% at distances of 20 mm from the center. The effective FOV, as seen from simulation, approximates a spherical shell of ~40 mm diameter, with a slight depression at its center.

Figure 5 shows T2-w imaging results at 3T for ICMRI in an ex-vivo Left Atrium (A, B) and in-vivo Right Atrium (C-G). The imaging-coil provided a $400\% \pm 30\%$ boost in apparent SNR over a $4 \times 4 \times 4$ cm³ FOV in the Left Atrium in the ex-vivo and in-vivo swine hearts. A boost of only $300 \pm 30\%$ occurred when the ICMRI shaft was oriented (± 5 degrees) along the magnet B_0 axis.

Figure 6A,B shows 3D GRE imaging results at 1.5T for ICMRI in a swine Right Atrium. The SNR of ICMRI

is compared to the combined 1.5T spine and cardiac arrays. A $510 \pm 30\%$ SNR boost was observed over a $5 \times 5 \times 5$ cm³ FOV. Figure 6C,D show the signals of the three MR-tracking coils on the expanded ICMRI tip, herein displayed without powering ON the imaging-coil, which is a fast way to determine tip location. By following their location over physiological cycles, these coils can also be used for motion compensation,³³ which can reduce motion blurring.

3.3 | Navigation Using the 3D Slicer Workstation

Using MR-Tracked navigation, the ICMRI guiding sheath was brought to the intra-atrial septum. ICMRI and the EP catheter were then passed into the Left Atrium through

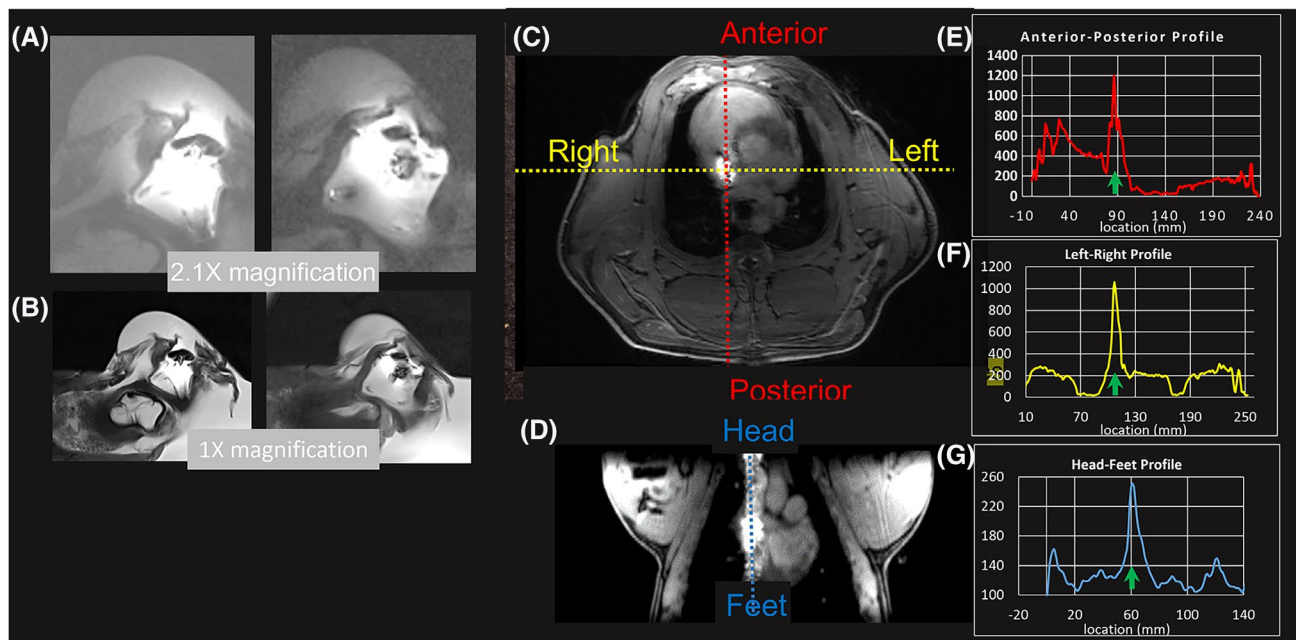


FIGURE 5 3T ICMRI imaging-coil SNR results ex-vivo and in-vivo. (A, B) T2-weighted FSE images from expanded imaging-coil in an ex-vivo pig left atrium, distanced from the surface arrays to emulate human conditions. (A) SNR of the IMCRI imaging-coil alone, and (B) in an array together with elements of the 32-coil 3T body and spine arrays. The ICMRI imaging-coil provided an SNR ratio of $400 \pm 30\%$ versus the surface coils over a $4 \times 4 \times 4 \text{ cm}^3$ FOV. (C, D) In-vivo axial and coronal GRE images taken with ICMRI navigated to a swine right atrium and then expanded. (E–G) Profiles along the Red, Yellow and Blue lines in (C, D) show the SNR ratios of the imaging-coil (center location indicated by green arrow) versus 32-channel surface-array elements. In the Anterior-Posterior direction, the imaging-coil gives a $460 \pm 40\%$ SNR ratio vs the surface arrays, in the Left-Right direction a $440 \pm 40\%$ SNR ratio and in the Head-Feet direction a $300 \pm 70\%$ SNR ratio, over a 4 cm length

a hole that had previously been made in the X-ray lab (Figure 7). Navigational experiments were performed with the two devices inside the left atrium, testing the ability to apply ICMRI tip deflection and use the 3–4 cm protruding EP catheter tip to reach all the pulmonary-vein ostia, as well as the left-atrial roof, as required for ablating persistent AF. By deflecting and rotating the guiding-sheath along with the ablation catheter, it was possible to reach all locations, which was not possible when using the ablation catheter alone. Figure 8A,B show the illumination that the expanded imaging-coil provides inside the Left Atrium, demonstrating that in the swine atrium, it is possible to leave ICMRI in a single location while moving around with the protruding EP catheter tip and mapping or ablating at multiple locations.

3.4 | Monitoring RF ablation using ICMRI's imaging-coil

In Experiment 1 (Figure 8A–D), ICMRI and the EP catheter were withdrawn from the left atrium into the right atrium. The EP catheter was used to make 6 ablation lesions (20 Watts for 90 s each) while slowly moving the catheter along the right atrial roof. Once ablation was

completed, the ICMRI tip was expanded and a $1 \times 1 \times 1 \text{ mm}^3$ -resolution TWILITE acquisition was performed. This acquisition was performed with the ICMRI coil alone, so that a restricted FOV (far smaller than required to image the entire heart) could be used, requiring fewer phase-encodes, and taking advantage of the enhanced SNR that the ICMRI tip coil offers. Figure 8C,D show the TWILITE and histology photo, respectively. It is apparent that the ablation procedure created both continuous and interspaced ablation lesions. We previously demonstrated¹¹ the ability to thereafter return to these precise locations with the EP catheter and close gaps between adjacent ablation lesions by applying additional RFA, which may reduce dramatically arrhythmia recurrence.

In Experiment 2 (Figure 8E–H), The ICMRI catheter was used to navigate to the RA, and the imaging-coil was opened immediately below the LA. The EP ablation catheter was then advanced into the LA through a trans-septal hole, and two ablation lesions created on the LA roof. Figures E–G show high-resolution TWILITE images (resolution = $0.8 \times 0.8 \times 1.0 \text{ mm}^3$) of the result, while H shows the gross histology result. It is apparent that two lesions were created with an extensive gap between them.

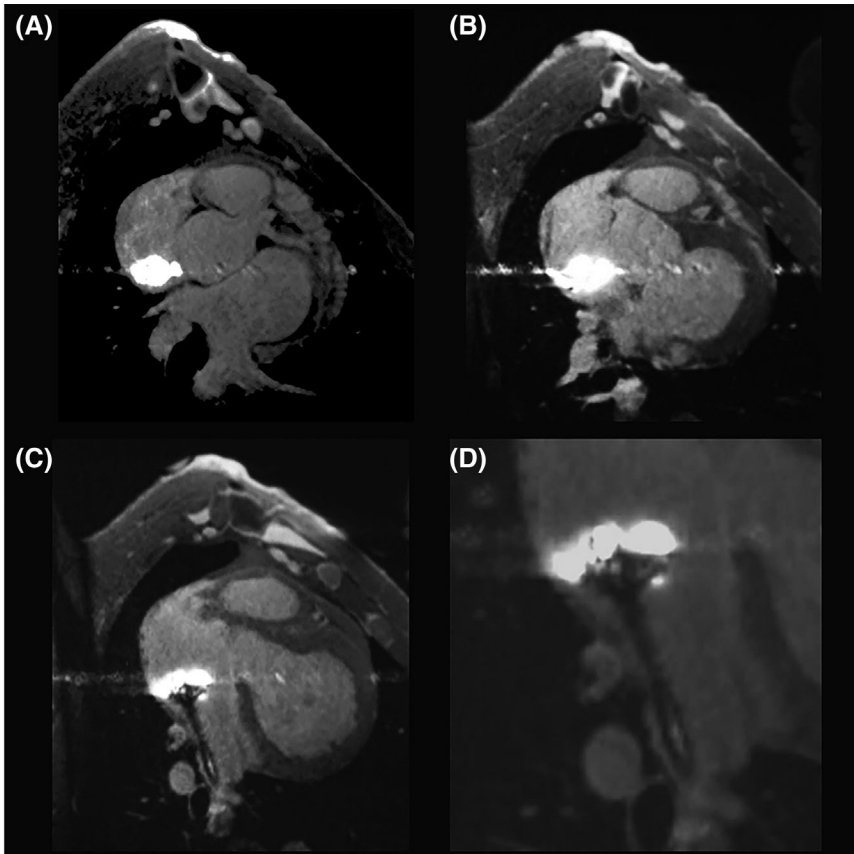


FIGURE 6 ICMRI deployed in the right ventricle at 1.5T. Respiratory-navigated & ECG-gated (trigger delay 432 ms) 3D GRE scan. ICMRI gave a $510 \pm 30\%$ SNR boost over the 32-channel spine & body arrays over a $5 \times 5 \times 5 \text{ cm}^3$ FOV). (A, B) Images of the ICMRI imaging-coil in the Right Ventricle, with only the ICMRI imaging-coil and the surface arrays enabled, demonstrate its strong signal (C, D) View of the signals from the MRT coils alone on the expanded ICMRI tip, performed by not powering ON the imaging-coil, demonstrates their ability to indicate the distal-tip location. In this tetrahedron configuration, the tracking-coils' location within physiological cycles can be tracked and used for imaging motion compensation. (D) Is an enlarged view of (C). The artifacts in B-D are Gibbs artifacts that result from the strong signal intensity of the local coils

4 | DISCUSSION

A deflectable metallic-braided sheath of 6 mm OD and 1 m length that is MRI-conditional at both 3T and 1.5T was constructed by employing MBaluns for heat amelioration. We believe this is the first large metallic guiding-sheath for use in the MR environment, which can potentially be used to deploy other ablative devices (Laser catheters, microwave antennas, focused ultrasound transducers, cryogenic catheters).

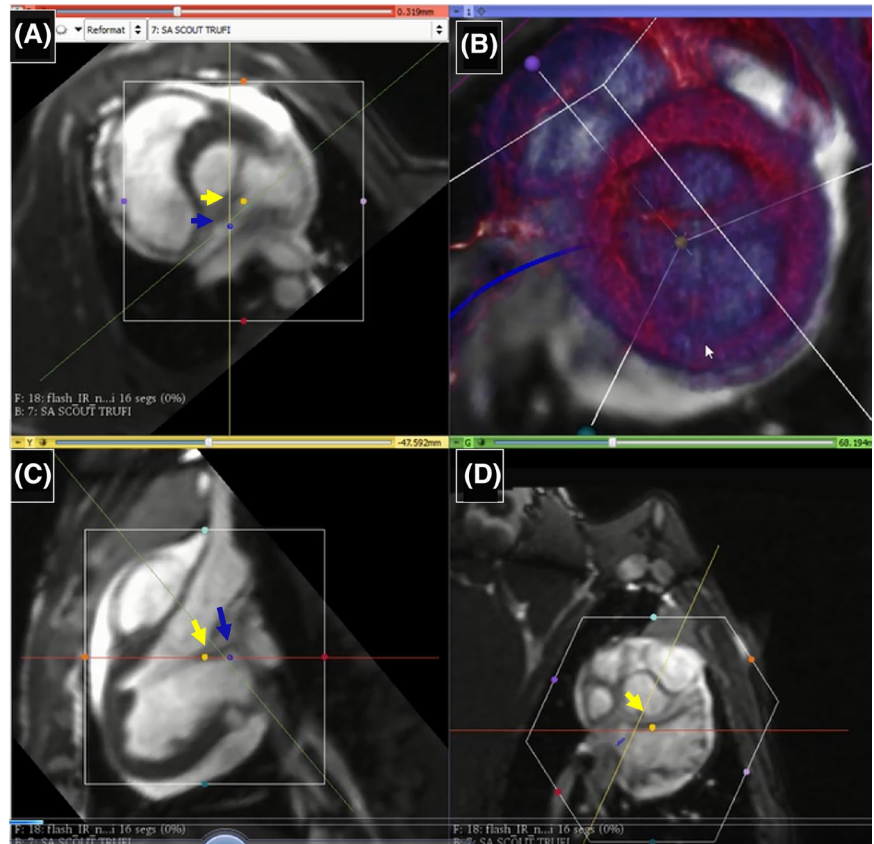
We also demonstrated the ability to add a miniature protected pre-amplifier circuit to the distal end of the sheath, utilizing sub-millimeter electronic-component dies that were wire-bonded together on an FPC. With this protected pre-amplifier, we were able to use an expandable imaging-coil without entailing the large ($>3 \text{ dB}$) SNR losses that result from use of micro-coaxial cables on ICMRI's long shaft. As a result, we were able to use the ICMRI expanded imaging-coil to obtain a 400%–500% boost in SNR in regions of $4 \times 4 \times 4 \text{ cm}^3$ size, which we employed to image acute ablation lesions faster. Such an enhancement is superior to that possible with advanced cardiac surface arrays,^{50,51} especially in the posterior heart, although ICMRI is only useful for interventional

procedures. We believe that this is the first experimental utilization of such a tip pre-amplifier, which may also be useful for other MR-guided cardiovascular procedures, especially for small-diameter elongated devices (guidewires, micro-catheters) where the coil inductance is inherently small, so the distal-end SNR is low, and is then reduced by use of thin coaxial lines, potentially disallowing accurate passive- or active-localization.

In addition, MRT coils were mounted on the expanding section. While folded, these were employed for active navigation of ICMRI and an internal EP catheter from the femoral veins to the right and left heart in 10 swine. When the ICMRI tip region is expanded, it should be possible to use the MRT coils for in-situ physiological motion-compensation of imaging,^{33,52} although this was not demonstrated in the present study.

To perform these studies, we developed an open-source 3D Slicer-based cardiovascular navigational workstation based on MR-Tracked input. The workstation is also able to display intracardiac (EGM) and surface ECG traces, as well as produce electroanatomic maps. We are currently working to allow the workstation to also use impedance-tracking, so that we can register electro-anatomical maps to MRI images, and navigate ICMRI outside the MRI scanner.

FIGURE 7 1.5T 3D Slicer workstation visualization. Display at a point during navigation, showing insertion of ICMRI, with folded imaging-coil and a protruding EP catheter, through a trans-septal hole into the Left Atrium. (A) short axis slice; (B): 3D view of ICMRI (blue) navigated into LA through the hole in the septum. Highlighted (red) structures are cardiac-chamber walls segmented from the SSFP data; (C): sagittal slice; (D): short-axis left atrial image. Yellow and blue points (highlighted with arrows) show the locations of two of the MR-tracking coils mounted on the ICMRI shaft. A video of navigation in a simulated human left atrium is shown in Supporting information Video S1.



To perform RF-ablation monitoring, we used the TWILITE sequence. It is currently an excellent method to predict thermal-ablation outcomes in areas where Proton Resonance Shift temperature mapping is difficult to use.^{53–55} We used the SNR that the ICMRI imaging-coil provides to reduce acquisition time to 5:30 min, without sacrificing image quality. The large discrepancy between the ICMRI imaging-coil and the surface-array intensity, in regions close to the ICMRI coil, may require application of pre-scan B1 normalization filters, provided by all MRI vendors, to properly scale the images according to their intensity before forming the combined-array images, removing artifacts resulting from the intensity differences (as seen in Figure 6).

Compressed sensing methods which take advantage of the improved SNR that ICMRI's imaging-coil affords to further accelerate imaging speed⁵⁶ were not investigated, but are planned for future studies.

We demonstrated the utility of the amplified ICMRI imaging-coil at both 1.5 and 3T. At present, interventional cardiovascular MRI is preferably performed at 1.5T due to the higher 3T motion sensitivity, higher micro-coax cable losses, and the higher rate of energy deposition. However, 3T use can become advantageous when imaging speed exceeds specific physiological temporal thresholds (one breathing cycle). This is easier to achieve with ICMRI since the heating risks are ameliorated with

MBaluns, and the higher SNR permits reducing scan durations. Future work will focus on investigating possible 3T advantages.

This study has limitations. We observed that an electrically-disconnected expanded ICMRI can result in 12°C (1.5T) or 14°C (3T) heating during 4 Watt/kg SAR sequences, when placed in regions lacking fluid circulation, which requires practicing caution when using ICMRI in its current state, such as folding the imaging-coil when it is not being used. However, even at 3T, use of an electrically connected ICMRI catheter in well-perfused cardiac chambers should be possible, since heating is limited to 1.8°C. Reducing heating further may require denser placement of MBaluns on the distal shaft, or continuously flowing fluid past this region (“irrigating”). Secondly, efficient use of ICMRI may require reducing strong intensity gradients in the images <5 mm from the imaging-coil with image intensity bias correction filters.⁵⁷ Thirdly, we did not demonstrate “real-time” (<15 sec/image) imaging during RFA primarily because attempts to perform that required use of low-resolution 2D imaging, which resulted in artifactual images, mainly due to variation of the lesion's plane between successive images. Fourthly, we did not employ the MR-Tracking coils for motion compensation in these animal studies, due to our software's current inability to turn ON and OFF selective coils in real-time.

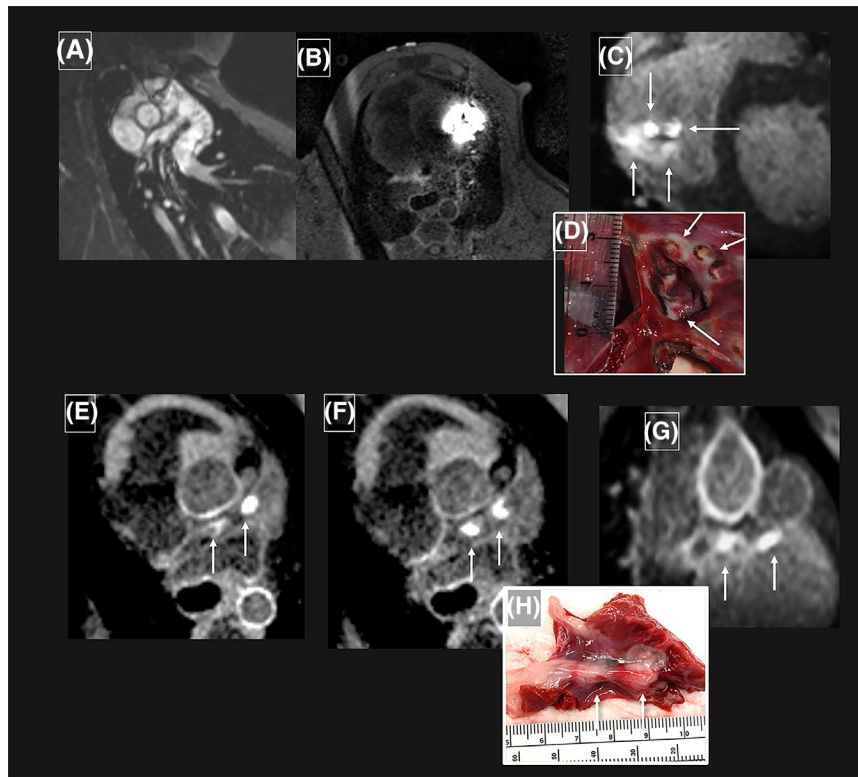


FIGURE 8 RF Ablation at 1.5T with ICMRI monitoring. Experiment1 (A-D). (A) The ICMRI guiding-sheath and an EP catheter are brought to the left atrium together. (B) ICMRI's imaging-coil is expanded in the LA and turned ON, demonstrating its image intensity, together with the surface arrays, relative to the surface arrays alone (what is observed further away from ICMRI). (C) ICMRI and the EP catheter were then pulled back into the right atrium, and ablation lesions created in the right atrial roof with the EP catheter (setting: 20 Watts for 90 s each). TWILITE was then performed with ICMRI alone in a 5:30 min $1 \times 1 \times 1 \text{ mm}^3$ resolution 14 cm FOV acquisition covering only the right atrium, showing the acute lesions created (white arrows), with ablation gaps visualized between some. (D) Histological photograph of the lesions. Experiment2 (E-H). An ICMRI catheter was advanced to the RA, and the imaging-coil expanded below the LA. The EP catheter was then advanced alone into the LA. Ablation lesions were created on the roof of the LA. TWILITE was then performed in a 7:0 min $0.8 \times 0.8 \times 1.0 \text{ mm}^3$ resolution 14 cm FOV acquisition, showing the acute lesions (white arrows). (E) and (F) are short axis views, (G) is a coronal view, and (H) Histological photograph of the lesions.

Finally, the shape of ICMRI's expandable section may need to change for work in the left ventricle, where there are multiple muscle tissues that protrude from the endocardial surface, and which may entangle the ICMRI tip.

ACKNOWLEDGMENTS

This study was supported by NIH U41-RR019703, U54-HL119145, R01-EB020667, R01-HL094610, AHA 10SDG261039, and grants from Abbott Laboratories. We thank Robert Aiken for help constructing this system.

CONFLICT OF INTEREST

Gregory Olson and Jeffrey Schweitzer are employees of Abbott Laboratories. Ehud J. Schmidt and Henry R. Halperin receive research and grant support from Abbott Laboratories.

ORCID

Ehud J. Schmidt  <https://orcid.org/0000-0002-5792-2087>
Akbar Alipour  <https://orcid.org/0000-0002-7981-6808>

REFERENCES

1. Nordbeck P, Quick HH, Bauer WR, Ertl G, Ladd ME, Ritter O. Initial clinical application of real-time MR imaging-guided ablation of cardiac arrhythmia in patients with atrial flutter. *Radiology*. 2014;273:310-311.
2. Grothoff M, Piorkowski C, Eitel C, et al. MR imaging-guided electrophysiological ablation studies in humans with passive catheter tracking: initial results. *Radiology*. 2014;271:695-702.
3. Eitel C, Hindricks G, Grothoff M, Gutberlet M, Sommer P. Catheter ablation guided by real-time MRI. *Curr Cardiol Rep*. 2014;16:511.
4. Chao TF, Tsao HM, Lin YJ, et al. Clinical outcome of catheter ablation in patients with nonparoxysmal atrial fibrillation: results of 3-year follow-up. *Circ Arrhythm Electrophysiol*. 2012;5:514-520.
5. Schmidt EJ, Halperin HR. MRI use for atrial tissue characterization in arrhythmias and for EP procedure guidance. *Int J Cardiovasc Imaging*. 2017;34:81-95.
6. Opolski G, Januszkiewicz L, Szczerba E, et al. Readmissions and repeat procedures after catheter ablation for atrial fibrillation. *Cardiol J*. 2015;22:630-636.
7. Galand V, Pavin D, Behar N, et al. Localization of gaps during redo ablations of paroxysmal atrial fibrillation: preferential

- patterns depending on the choice of cryoballoon ablation or radiofrequency ablation for the initial procedure. *Arch Cardiovasc Dis.* 2016;109:591-598.
8. Bisbal F, Guiu E, Cabanas-Grandio P, et al. CMR-guided approach to localize and ablate gaps in repeat AF ablation procedure. *JACC Cardiovasc Imaging.* 2014;7:653-663.
 9. Guttman MA, Tao S, Fink S, Kolandaivelu A, Halperin HR, Herzka DA. Non-contrast-enhanced T1-weighted MRI of myocardial radiofrequency ablation lesions. *Magn Reson Med.* 2018;79:879-889.
 10. Tao S, Guttman MA, Fink S, et al. Ablation lesion characterization in scarred substrate assessed using cardiac magnetic resonance. *JACC Clin Electrophysiol.* 2019;5(1):91-100.
 11. Guttman MA, Tao S, Fink S, et al. Acute enhancement of necrotic radio-frequency ablation lesions in left atrium and pulmonary vein ostia in swine model with non-contrast-enhanced T1-weighted MRI. *Magn Reson Med.* 2020;83:1368-1379.
 12. Bisbal F, Benito E, Teis A, et al. Magnetic resonance imaging-guided fibrosis ablation for the treatment of atrial fibrillation: the ALICIA Trial. *Circ Arrhythm Electrophysiol.* 2020;13:e008707.
 13. Enriquez A, Saenz LC, Rosso R, et al. Use of intracardiac echocardiography in interventional cardiology: working with the anatomy rather than fighting it. *Circulation.* 2018;137:2278-2294.
 14. Enriquez A, Tapias C, Rodriguez D, et al. Role of intracardiac echocardiography for guiding ablation of tricuspid valve arrhythmias. *HeartRhythm Case Rep.* 2018;4:209-213.
 15. Schnall MD, Lenkinski RE, Pollack HM, Imai Y, Kressel HY. Prostate: MR imaging with an endorectal surface coil. *Radiology.* 1989;172:570-574.
 16. Krieger A, Susil RC, Menard C, et al. Design of a novel MRI compatible manipulator for image guided prostate interventions. *IEEE Trans Biomed Eng.* 2005;52:306-313.
 17. Shunk KA, Lima JA, Heldman AW, Atalar E. Transesophageal magnetic resonance imaging. *Magn Reson Med.* 1999;41:722-726.
 18. Eryaman Y, Oner Y, Atalar E. Design of internal MRI coils using ultimate intrinsic SNR. *Magn Reson Mater Phys Biol Med.* 2009;22:221-228.
 19. Serfaty JM, Yang X, Aksit P, Quick HH, Solaiyappan M, Atalar E. Toward MRI-guided coronary catheterization: visualization of guiding catheters, guidewires, and anatomy in real time. *J Magn Reson Imaging.* 2000;12:590-594.
 20. Qiu B, Gao F, Karmarkar P, Atalar E, Yang X. Intracoronary MR imaging using a 0.014-inch MR imaging-guidewire: toward MRI-guided coronary interventions. *J Magn Reson Imaging.* 2008;28:515-518.
 21. Worthley SG, Helft G, Fuster V, et al. A novel nonobstructive intravascular MRI coil: in vivo imaging of experimental atherosclerosis. *Arterioscler Thromb Vasc Biol.* 2003;23:346-350.
 22. Martin AJ, McLoughlin RF, Chu KC, Barberi EA, Rutt BK. An expandable intravenous RF coil for arterial wall imaging. *J Magn Reson Imaging.* 1998;8:226-234.
 23. Sathyanarayana S, Schar M, Kraitchman DL, Bottomley PA. Towards real-time intravascular endoscopic magnetic resonance imaging. *JACC Cardiovasc Imaging.* 2010;3:1158-1165.
 24. Erturk MA, El-Sharkawy AM, Moore J, Bottomley PA. 7 Tesla MRI with a transmit/receive loopless antenna and B1-insensitive selective excitation. *Magn Reson Med.* 2014;72:220-226.
 25. OwenDuffy.net. *RF Coaxial Transmission Line Loss Calculator.* 2021 ed. Owen Duffy; 2021. <https://owenduffy.net/calc/tl/cllc.htm>. Accessed October 10, 2021.
 26. Yak N, Anderson KJ, Wright GA. Tuning and amplification strategies for intravascular imaging coils. *Magn Reson Med.* 2012;68:1675-1680.
 27. AmericanRadioRelayLeague. In: H. Silver, ed. *The ARRL Handbook for Radio Communications.* 2012 ed. National Association for Amateur radio (American Radio Relay League); 2012. <https://www.arrl.org>. Accessed October 10, 2021.
 28. Axon-Cables.com. Picocoax miniature coaxial cables. 2002.
 29. Alipour A, Schmidt EJ, Kolandaivelu A, et al. Abstract 13680: preclinical validation of a device-set of impedance- and magnetic resonance tracked metallic devices for conventional and Mr-guided electrophysiological intervention. *Circulation.* 2019;140(S1):A13680-A13680.
 30. Bouzas-Mosquera A, Brouillon FJ, Alvarez-Garcia N, et al. Left atrial size and risk for all-cause mortality and ischemic stroke. *Can Med Assoc J.* 2011;183:E657-E664.
 31. Mansour M, Refaat M, Heist EK, et al. Three-dimensional anatomy of the left atrium by magnetic resonance angiography: implications for catheter ablation for atrial fibrillation. *J Cardiovasc Electrophysiol.* 2006;17:719-723.
 32. Sanchez-Quintana D, Lopez-Minguez JR, Macias Y, Cabrera JA, Saremi F. Left atrial anatomy relevant to catheter ablation. *Cardiol Res Pract.* 2014;2014:289720.
 33. de Arcos RJ, Dabaghyan M, Stevenson WG, et al. ISMRM abstract 5558: Motion-corrected high-resolution intra-cardiac imaging using MR-Tracking coils: reducing the effect of noise on motion estimation. Proc. ISMRM 25, Honolulu, HI; 2017. Abstract A5558.
 34. Qin L, Schmidt EJ, Hoge WS, et al. Prospective motion correction for intra-cardiac MRI using a tetrahedron-shaped array of MR-tracking coils. *Circulation.* 2010;122:A10424.
 35. Taylor AJ, Tse ZT, Schmidt EJ, Miller M, Fok MP, Nilsson K. Applying origami coil design for deployable intra-cardiac MRI catheter. Proc. Intl. Soc. Mag. Res. Med. 24th annual meeting Singapore 2016. Abstract 3122. <https://cds.ismrm.org/protected/16MPresentations/abstracts/3122.html>. Accessed February 2, 2022.
 36. Chen Y, Zion ZT, Wang W, Kwong RY, Stevenson WG, Schmidt EJ. Intra-cardiac MR imaging & MR-tracking catheter for improved MR-guided EP. *JCMR.* 2015;17(Suppl 1):1-3. doi: 10.1186/1532-429X-17-S1-P237
 37. Alipour A, Meyer ES, Dumoulin CL, et al. MRI conditional actively tracked metallic electrophysiology catheters and guidewires with miniature tethered radio-frequency traps: theory, design, and validation. *IEEE Trans Biomed Eng.* 2020;67:1616-1627.
 38. Dumoulin CL, Mallozzi RP, Darrow RD, Schmidt EJ. Phase-field dithering for active catheter tracking. *Magn Reson Med.* 2010;63:1398-1403.
 39. Chen Y, Wang W, Schmidt EJ, et al. Design and fabrication of MR-tracked metallic stylet for gynecologic brachytherapy. *IEEE/ASME Trans Mech.* 2016;21:956-962.
 40. Wang W, Dumoulin CL, Viswanathan AN, et al. Real-time active MR-tracking of metallic stylets in MR-guided radiation therapy. *Magn Reson Med.* 2015;73:1803-1811.
 41. Schmidt EJ, Tse ZT, Reichlin TR, et al. Voltage-based device tracking in a 1.5 tesla MRI during imaging: initial validation in swine models. *Magn Reson Med.* 2014;71:1197-1209.
 42. Wittkamp FH, Wever EF, Derksen R, et al. LocaLisa: new technique for real-time 3-dimensional localization of regular intracardiac electrodes. *Circulation.* 1999;99:1312-1317.
 43. Fedorov A, Beichel R, Kalpathy-Cramer J, et al. 3D Slicer as an image computing platform for the quantitative imaging network. *Magn Reson Imaging.* 2012;30:1323-1341.

44. IEC. *IEC 60601-2-33 Medical Electrical Equipment—Part 2-33: Particular Requirements for the Safety of Magnetic Resonance Equipment for Medical Diagnosis*. Zurich, Switzerland: International Electrotechnical Commission; 2010. <https://webstore.iec.ch/publication/2647>. Accessed October 10, 2021.
45. Dabaghyan M, De Arcos RJ, Kwong R, et al. MRI-Compatible Voltage Device Tracking (VDT) Navigation: Simultaneous Tracking and Imaging with High-Gradient-Duty-Cycle Sequences via Complete Removal of Gradient Induced Voltages: Initial Results. *Proc. ISMRM 25th Annual Meeting & Exhibition*; April 22-27, 2017; Honolulu, HI. Abstract 5552.
46. Lorensen WE, Cline HE. Marching cubes: a high resolution 3D surface construction algorithm. *SIGGRAPH 1987: Proceedings 14th annual conference on Computer graphics and interactive techniques*. 1987;21:163-169.
47. Tokuda J, Fischer GS, Papademetris X, et al. OpenIGTLink: an open network protocol for image-guided therapy environment. *the international journal of medical robotics ± computer assisted surgery*. *MRCAS*. 2009;5:423-434.
48. ASTM-International. ASTM F2182-19e2: Standard Test Method for Measurement of Radio Frequency Induced Heating on or Near Passive Implants during Magnetic Resonance Imaging. 2020. doi: 10.1520/F2182-19E02
49. Alipour A, Schmidt EJ, Koldaiveilu A, et al. Preclinical validation of a device-set of impedance- and magnetic resonance tracked metallic devices for conventional and MR-guided electrophysiological intervention. *Circulation*. 2019;140:A13680.
50. Etzel R, Mekkaoui C, Ivshina ES, et al. Optimized 64-channel array configurations for accelerated simultaneous multislice acquisitions in 3T cardiac MRI. *Magn Reson Med*. 2021;86:2276-2289.
51. Schmitt M, Potthast A, Sosnovik DE, et al. A 128-channel receive-only cardiac coil for highly accelerated cardiac MRI at 3 Tesla. *Magn Reson Med*. 2008;59:1431-1439.
52. Qin L, Schmidt E, Hoge WS, et al. Prospective motion correction for intra-cardiac MRI using a tetrahedron-shaped array of MR-tracking coils. *Circulation*. 2010;122(S21):A10424. https://www.ahajournals.org/doi/10.1161/circ.122.suppl_21.A10424. Accessed October 10, 2021.
53. Ozenne V, Toupin S, Bour P, et al. Improved cardiac magnetic resonance thermometry and dosimetry for monitoring lesion formation during catheter ablation. *Magn Reson Med*. 2017;77:673-683.
54. Winter L, Oberacker E, Paul K, et al. Magnetic resonance thermometry: methodology, pitfalls and practical solutions. *Int J Hypertherm*. 2016;32:63-75.
55. de Senneville BD, Roujol S, Jais P, Moonen CT, Herigault G, Quesson B. Feasibility of fast MR-thermometry during cardiac radiofrequency ablation. *NMR Biomed*. 2012;25:556-562.
56. Sanders JW, Song H, Frank SJ, et al. Parallel imaging compressed sensing for accelerated imaging and improved signal-to-noise ratio in MRI-based postimplant dosimetry of prostate brachytherapy. *Brachytherapy*. 2018;17:816-824.
57. Tustison NJ, Avants BB, Cook PA, et al. N4ITK: improved N3 bias correction. *IEEE Trans Med Imaging*. 2010;29:1310-1320.

SUPPORTING INFORMATION

Additional supporting information may be found in the online version of the article at the publisher's website.

FIGURE S1 Circuit diagrams, components and vendors. (A) Circuit of the “star” shaped imaging-coil, the embedded capacitors for tuning and matching and the high-voltage pin-diode protected distal LNA. The diodes, tuning and matching capacitors, and LNA were located on one of the five struts of the imaging-coil. (B) Circuit of the MR conditional Bias-T circuit, which is required to power the LNA. The Bias-T was located in a separate RF-shielded box attached to the handle of the ICMRI catheter by 40 cm long coaxial cables mounted with 2 Baluns. (C) Circuit for tuning, matching and passive decoupling of an MR-tracking coil. Five of these circuits were in the separate RF-shielded box, also used for (B).

FIGURE S2 Electromagnetic simulation of the expanded ICMRI imaging-coil radio-frequency field (B_1^-) at 1.5T. (A1) The EM simulation set-up, showing the ICMRI imaging-coil inside a cylinder of simulated blood solution. (A2) CAD model of the imaging-coil, showing the series embedded capacitors and the dual-winded pattern. (B, C) B_1^- along planes parallel to the coil at the center and 5 mm below center. (D-F) B_1^- along planes perpendicular to the coil. The expanded coil has a pentagram-shaped in-plane radiation pattern, with the maximal B_1^- (B) observed in the center plane close to the coil windings, with a 26% drop in amplitude in a 5 mm-diameter region at the center. In planes perpendicular to the coil plane, the amplitude (D-F) drops by 50% at distances of 20 mm from the center. The effective FOV, as seen from the simulation, approximates a spherical shell of ~40 mm diameter, with a slight lull in its center.

VIDEO S1 Video showing MR-tracked navigation of the ICMRI deflectable sheath (Brown) and a protruding deflectable EP catheter (Blue) inside a human-sized LA model (Abbott laboratories) filled with saline solution, which was placed within a human-sized torso phantom (dimensions: SI = 50 cm, LR = 40 cm, AP = 35 cm) showing access to several PV ostia and the LA roof, with the MR-Tracked electrodes on the shafts shown as Grey rings. Tracking Data transferred at 100 Mbyte/s from the 1.5T MRI to 3D Slicer workstation. Navigation was performed on a simultaneous display of 2 anatomic orientations, which were displayed on an MR-conditional monitor in the MRI suite. MR-Tracking rate was 16 fps, $0.9 \times 0.9 \times 0.9 \text{ mm}^3$ resolution.

How to cite this article: Schmidt EJ, Olson G, Tokuda J, et al. Intracardiac MR imaging (ICMRI) guiding-sheath with amplified expandable-tip imaging and MR-tracking for navigation and arrhythmia ablation monitoring: Swine testing at 1.5 and 3T. *Magn Reson Med*. 2022;87:2885–2900. doi:[10.1002/mrm.29168](https://doi.org/10.1002/mrm.29168)